

Odd-frequency Pairs and Josephson Current through a Strong Ferromagnet

Yasuhiro Asano

Department of Applied Physics, Hokkaido University, Sapporo 060-8628, Japan

Yuki Sawa and Yukio Tanaka

CREST-JST and Department of Applied Physics, Nagoya University, Nagoya 464-8603, Japan

Alexander A. Golubov

Faculty of Science and Technology, University of Twente, 7500 AE, Enschede, The Netherlands

(Dated: November 4, 2021)

We study Josephson current in superconductor / diffusive ferromagnet /superconductor junctions by using the recursive Green function method. When the exchange potential in a ferromagnet is sufficiently large as compared to the pair potential in a superconductor, an ensemble average of Josephson current is much smaller than its mesoscopic fluctuations. The Josephson current vanishes when the exchange potential is extremely large so that a ferromagnet is half-metallic. Spin-flip scattering at junction interfaces drastically changes the characteristic behavior of Josephson current. In addition to spin-singlet Cooper pairs, equal-spin triplet pairs penetrate into a half metal. Such equal-spin pairs have an unusual symmetry property called odd-frequency symmetry and carry the Josephson current through a half metal. The penetration of odd-frequency pairs into a half metal enhances the low energy quasiparticle density of states, which could be detected experimentally by scanning tunneling spectroscopy. We will also show that odd-frequency pairs in a half metal cause a nonmonotonic temperature dependence of the critical Josephson current.

PACS numbers: 74.50.+r, 74.25.Fy,74.70.Tx

I. INTRODUCTION

Ferromagnetism and spin-singlet superconductivity are competing orders because the exchange potential breaks down spin-singlet pairs. Spin-singlet pairs, however, do not always disappear under the influence of an exchange potential. Long time ago Fulde-Ferrell¹ and Larkin-Ovchinnikov² discussed inhomogeneous spin-singlet superconductivity in the presence of an exchange potential. It was shown that the superconducting order parameter oscillates in real space because the exchange potential shifts the center-of-mass momentum of a Cooper pair. Similarly, a Cooper pair has been discussed in superconductor / ferromagnet (SF) and superconductor / ferromagnet / superconductor (SFS) junctions^{3,4,5,6,7,8,9,10}. These studies showed that a pairing function in a ferromagnet changes its sign periodically in real space. As a consequence, SFS junctions may undergo so-called $0-\pi$ transition with varying length of a ferromagnet or temperature.

Previous theoretical studies of the proximity effect in a ferromagnet were mainly based on solving the quasiclassical Usadel equations¹¹ valid when the exchange potential V_{ex} is comparable to or smaller than the pair potential in a superconductor at zero temperature Δ_0 . Cooper pairs can penetrate into a ferromagnet within a short distance $\xi_h = \sqrt{D/V_{ex}}$, where D is the diffusion constant in a ferromagnet. Thus, penetration of spin-singlet Cooper pairs into a ferromagnet with large V_{ex} would be impossible and the Josephson coupling via such a strong ferromagnet would be vanishingly small. A recent experiment¹², however, demonstrated the existence

of Josephson coupling through a strong ferromagnet with $V_{ex} \gg \Delta_0$. In addition to this, the experiment¹³ has even shown Josephson coupling in superconductor / half metal / superconductor (S/HM/S) junctions. A half metal is an extreme case of a completely spin polarized material because its electronic structure is insulating for one spin direction and metallic for the other. Thus one has to seek a new state of Cooper pairs in a strong ferromagnet. The experiment by Keizer et. al. has motivated a number of theoretical studies in this direction^{14,15,16,17}.

Prior to the experiment¹³, Eschrig *et.al.*¹⁸ have addressed this challenging issue. In the *clean limit*, they have shown that p -wave spin-triplet pairs induced by spin-flip scattering at a junction interface can carry Josephson current. In practical S/HM/S junctions, however, a half metal is close to the *dirty limit* in the diffusive transport regime; the elastic mean free path ℓ may be smaller or comparable to the coherence length and is much smaller than the size of the half metal L_N . Thus, the effects of the impurity potential on the Josephson current should be clarified in a SFS junction consisting of a strong ferromagnet. In this paper, we discuss the Josephson effect in SFS junctions for arbitrary magnitude of V_{ex} . When V_{ex} is much larger than Δ_0 , an ensemble average of the Josephson current is much smaller than its mesoscopic fluctuations^{19,20}. Fluctuations of the pairing function in a ferromagnet is responsible for the large fluctuations of Josephson current. The Josephson current vanishes in S/HM/S in the absence of spin-flip scattering at junction interfaces. Spin-flip scattering at junction interfaces drastically changes the characteristic behavior of Josephson current and properties of Cooper

pairs in a ferromagnet. Spin-flip scattering allows for the penetration of equal-spin-triplet Cooper pairs which have unusual symmetry property called odd-frequency symmetry⁶. When the contribution of equal-spin-triplet Cooper pairs to the Josephson current is dominant, the self-averaging property of the Josephson current is recovered. In particular in diffusive S/HM/S junctions, all Cooper pairs in a half metal are in the odd-frequency equal-spin-triplet pairing state¹⁴. We also discuss local density of states in a ferromagnet which reflects the existence of odd-frequency Cooper pairs. A part of this study has been already published elsewhere¹⁴. Throughout this paper, we use the unit of $\hbar = k_B = 1$, where k_B is the Boltzmann constant.

This paper is organized as follows. In Sec. II, we explain the model of SFS junctions on two-dimensional tight-binding lattice and the method of calculation. The characteristic features of Josephson current in SFS junctions are discussed in Sec. III. In Sec. IV, we introduce spin-flip scattering at junction interfaces and discuss symmetry properties of Cooper pairs in a ferromagnet. We propose an experiment to observe odd-frequency pairs in SFS junctions based on calculated results of local density of states in Sec. V. The conclusions are formulated in Sec. VI.

II. MODEL

Let us consider the two-dimensional tight-binding model as shown in Fig. 1(a). A vector $\mathbf{r} = j\mathbf{x} + m\mathbf{y}$ indicates a lattice site, where \mathbf{x} and \mathbf{y} are unit vectors in the x and y directions, respectively. A junction consists of five segments: a ferromagnet ($3 \leq j \leq L_N - 2$), two thin ferromagnetic layers ($j = 1, 2, L_N - 1$, and L_N), and two superconductors ($-\infty \leq j \leq 0$ and $L_N + 1 \leq j \leq \infty$). In the y direction, the number of lattice sites is W and we assume a periodic boundary condition. Electronic states in a superconducting junction are described by the mean-field Hamiltonian

$$H_{\text{BCS}} = \frac{1}{2} \sum_{\mathbf{r}, \mathbf{r}'} \left[\tilde{c}_{\mathbf{r}}^\dagger h_{\mathbf{r}, \mathbf{r}'} \tilde{c}_{\mathbf{r}'} - \tilde{c}_{\mathbf{r}}^\dagger h_{\mathbf{r}, \mathbf{r}'}^* \left\{ \tilde{c}_{\mathbf{r}'}^\dagger \right\}^t \right] + \frac{1}{2} \sum_{\mathbf{r}, \mathbf{r}' \in \text{S}} \left[\tilde{c}_{\mathbf{r}}^\dagger \hat{\Delta}_{\mathbf{r}, \mathbf{r}'} \left\{ \tilde{c}_{\mathbf{r}'}^\dagger \right\}^t - \left\{ \tilde{c}_{\mathbf{r}} \right\}^t \hat{\Delta}_{\mathbf{r}, \mathbf{r}'}^* \tilde{c}_{\mathbf{r}'} \right], \quad (1)$$

$$\hat{h}_{\mathbf{r}, \mathbf{r}'} = [-t\delta_{|\mathbf{r}-\mathbf{r}'|, 1} + (\epsilon_{\mathbf{r}} - \mu + 4t)\delta_{\mathbf{r}, \mathbf{r}'}] \hat{\sigma}_0 - \mathbf{V}(\mathbf{r}) \cdot \hat{\boldsymbol{\sigma}} \delta_{\mathbf{r}, \mathbf{r}'}, \quad (2)$$

$$\hat{\Delta}_{\mathbf{r}, \mathbf{r}'} = e^{i\varphi_j} i\Delta \hat{\sigma}_2 \delta_{\mathbf{r}, \mathbf{r}'}, \quad (3)$$

$$\tilde{c}_{\mathbf{r}} = \begin{pmatrix} c_{\mathbf{r}, \uparrow} \\ c_{\mathbf{r}, \downarrow} \end{pmatrix}, \quad \left\{ \tilde{c}_{\mathbf{r}} \right\}^t = (c_{\mathbf{r}, \uparrow}, c_{\mathbf{r}, \downarrow}), \quad (4)$$

where $c_{\mathbf{r}, \sigma}^\dagger$ ($c_{\mathbf{r}, \sigma}$) is the creation (annihilation) operator of an electron at \mathbf{r} with spin $\sigma = (\uparrow \text{ or } \downarrow)$, S in the summation means superconductors, $\hat{\sigma}_j$ with $j = 1 - 3$ are the Pauli matrices, and $\hat{\sigma}_0$ is the 2×2 unit matrix. The

hopping integral t is considered among the nearest neighbor sites. In a ferromagnet, on-site potential is given

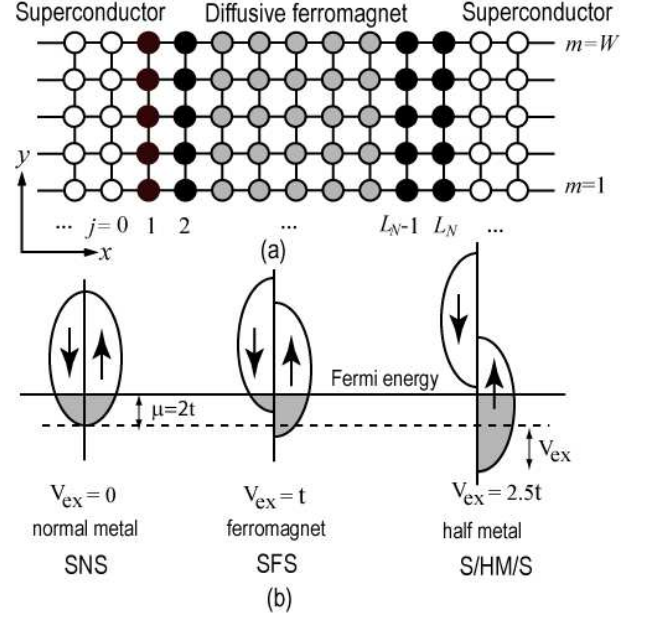


FIG. 1: (Color online) (a) A schematic figure of a SFS junction on tight-binding lattice. (b) Density of states for each spin direction. The Josephson junction is of the SNS, SFS, and S/HM/S type for $V_{\text{ex}}/t = 0, 1$ and 2.5 , respectively.

randomly in a range of $-V_I/2 \leq \epsilon_{\mathbf{r}} \leq V_I/2$, where we take the probability distribution for $\epsilon_{\mathbf{r}}$ uniform on this interval, and $\epsilon_{\mathbf{r}}$ at different points are uncorrelated. The uniform exchange potential in a ferromagnet is given by $\mathbf{V}(\mathbf{r}) = V_{\text{ex}}\mathbf{e}_3$, where \mathbf{e}_l for $l = 1 - 3$ is a unit vector in spin space. The Fermi energy μ is set to be $2t$ in a normal metal with $V_{\text{ex}} = 0$, while a ferromagnet and a half metal are respectively described by $V_{\text{ex}}/t = 1$ and 2.5 as shown in Fig. 1(b). Spin-flip scattering is introduced at $j = 1, 2, L_N - 1$, and L_N , where we choose $\mathbf{V}(\mathbf{r}) = V_S\mathbf{e}_2$. In a superconductor, we take $\epsilon_{\mathbf{r}} = 0$ and Δ is an amplitude of the pair potential in s -wave symmetry. The macroscopic phases are given by $\varphi_j = \varphi_L$ in the left superconductor and by $\varphi_j = \varphi_R$ in the right one.

The Hamiltonian is diagonalized by the Bogoliubov transformation,

$$\begin{bmatrix} \tilde{c}_{\mathbf{r}} \\ \left\{ \tilde{c}_{\mathbf{r}}^\dagger \right\}^t \end{bmatrix} = \sum_{\lambda} \begin{bmatrix} \hat{u}_{\lambda}(\mathbf{r}) & \hat{v}_{\lambda}^*(\mathbf{r}) \\ \hat{v}_{\lambda}(\mathbf{r}) & \hat{u}_{\lambda}^*(\mathbf{r}) \end{bmatrix} \begin{bmatrix} \tilde{\gamma}_{\lambda} \\ \left\{ \tilde{\gamma}_{\lambda}^\dagger \right\}^t \end{bmatrix}, \quad (5)$$

$$\tilde{\gamma}_{\lambda} = \begin{pmatrix} \gamma_{\lambda, \uparrow} \\ \gamma_{\lambda, \downarrow} \end{pmatrix}, \quad (6)$$

where $\gamma_{\lambda, \sigma}^\dagger$ ($\gamma_{\lambda, \sigma}$) is the creation (annihilation) operator of a Bogoliubov quasiparticle. The wave functions, \hat{u}_{λ} and \hat{v}_{λ} , satisfy the Bogoliubov-de Gennes equation²¹,

$$\sum_{\mathbf{r}'} \begin{bmatrix} \hat{h}_{\mathbf{r}, \mathbf{r}'} & \hat{\Delta}_{\mathbf{r}, \mathbf{r}'} \\ -\hat{\Delta}_{\mathbf{r}, \mathbf{r}'}^* & -\hat{h}_{\mathbf{r}, \mathbf{r}'}^* \end{bmatrix} \begin{bmatrix} \hat{u}_{\lambda}(\mathbf{r}') \\ \hat{v}_{\lambda}(\mathbf{r}') \end{bmatrix} = \begin{bmatrix} \hat{u}_{\lambda}(\mathbf{r}) \\ \hat{v}_{\lambda}(\mathbf{r}) \end{bmatrix} \hat{E}_{\lambda}. \quad (7)$$

The eigen value matrix \hat{E}_λ is diagonal and depends on spin channels. To solve the Bogoliubov-de Gennes equation, we apply the recursive Green function method^{22,23}. In this method, we calculate the Matsubara Green function

$$\check{G}_{\omega_n}(\mathbf{r}, \mathbf{r}') = \sum_{\lambda} \begin{bmatrix} \hat{u}_{\lambda}(\mathbf{r}) \\ \hat{v}_{\lambda}(\mathbf{r}) \end{bmatrix} [i\omega_n - \hat{E}_{\lambda}]^{-1} \begin{bmatrix} \hat{u}_{\lambda}^{\dagger}(\mathbf{r}') \\ \hat{v}_{\lambda}^{\dagger}(\mathbf{r}') \end{bmatrix} + \begin{bmatrix} \hat{v}_{\lambda}^*(\mathbf{r}) \\ \hat{u}_{\lambda}^*(\mathbf{r}) \end{bmatrix} [i\omega_n + \hat{E}_{\lambda}]^{-1} \begin{bmatrix} \hat{v}_{\lambda}^t(\mathbf{r}') \\ \hat{u}_{\lambda}^t(\mathbf{r}') \end{bmatrix}, \quad (8)$$

$$= \begin{pmatrix} \hat{g}_{\omega_n}(\mathbf{r}, \mathbf{r}') & \hat{f}_{\omega_n}(\mathbf{r}, \mathbf{r}') \\ -\hat{f}_{\omega_n}^*(\mathbf{r}, \mathbf{r}') & -\hat{g}_{\omega_n}^*(\mathbf{r}, \mathbf{r}') \end{pmatrix}, \quad (9)$$

where $\omega_n = (2n + 1)\pi T$ is a Matsubara frequency, n is an integer number, and T is the temperature. The Josephson current is given by

$$J = -ietT \sum_{\omega_n} \sum_{m=1}^W \text{Tr} [\check{G}_{\omega_n}(\mathbf{r}', \mathbf{r}) - \check{G}_{\omega_n}(\mathbf{r}, \mathbf{r}')] \quad (10)$$

with $\mathbf{r}' = \mathbf{r} + \mathbf{x}$. In this paper, 2×2 and 4×4 matrices are indicated by $\hat{\cdot}$ and $\check{\cdot}$, respectively.

In simulations, we first compute the Josephson current for a single sample with a specific random impurity configuration. After calculating the Josephson current over a number of different samples, an ensemble average of the Josephson current and its fluctuations are obtained as

$$\langle J \rangle = \frac{1}{N_s} \sum_{i=1}^{N_s} J_i, \quad (11)$$

$$\delta J = \sqrt{\langle J^2 \rangle - \langle J \rangle^2}, \quad (12)$$

where J_i is the Josephson current in the i th sample and N_s is the number of samples. Strictly speaking, N_s should be taken to be infinity. In this paper, we increase N_s until sufficient convergence of $\langle J \rangle$ and δJ is obtained. In the following, N_s is typically taken to be 100-2000.

To study the characteristics of Cooper pairs in a ferromagnet, we also analyze the anomalous Green function in Eq. (9). The pairing function is defined by the anomalous Green function and is decomposed into four components,

$$\sum_{\omega_c < \omega_n < \Delta_0} \frac{1}{W} \sum_{m=1}^W \hat{f}_{\omega_n}(\mathbf{r}, \mathbf{r}) = i \sum_{\nu=0}^3 f_{\nu}(j) \hat{\sigma}_{\nu} \hat{\sigma}_2, \quad (13)$$

where $\mathbf{r} = j\mathbf{x} + m\mathbf{y}$, $\omega_c = 0.01\Delta_0$ is a low energy cut-off and the pairing functions are averaged over whole lattice sites at j before ensemble averaging. In Eq. (13), $f_0(f_3)$ is the pairing function of spin-singlet (spin-triplet) pairs with spin structure of $(|\uparrow\downarrow\rangle - (+)|\downarrow\uparrow\rangle)/\sqrt{2}$. The pairing functions of $|\uparrow\uparrow\rangle$ and $|\downarrow\downarrow\rangle$ pairs are given by $f_{\uparrow\uparrow} = if_2 - f_1$ and $f_{\downarrow\downarrow} = if_2 + f_1$, respectively.

The quasiclassical Green function method^{11,24} is a powerful tool to study the proximity effect when the pair potential is much smaller than the Fermi energy. The

quasiclassical Green function, however, cannot be constructed in a half metal because the Fermi energy for one spin direction is no longer much larger than the pair potential. On the other hand, there is no such difficulty in our method. These are advantages of the recursive Green function method. Throughout this paper we fix the following parameters: $L_N = 74$, $W = 25$, $\mu = 2t$, and $V_I = 2t$. This parameter choice corresponds to the diffusive transport regime in the N, F and HM layers²⁵. The results presented below are not sensitive to variations of these parameters.

III. SFS JUNCTION WITHOUT SPIN-ACTIVE INTERFACE

In this section, we do not consider spin-flip scattering at the interfaces, (i.e., $V_S = 0$). We first discuss the Josephson current in SFS junctions as shown in Fig. 2, where $T = 0.1T_c$, $\Delta_0 = 0.01t$, T_c is the superconducting transition temperature, and the phase difference across a junction $\varphi = \varphi_L - \varphi_R$ is fixed at $\pi/2$. The presented re-

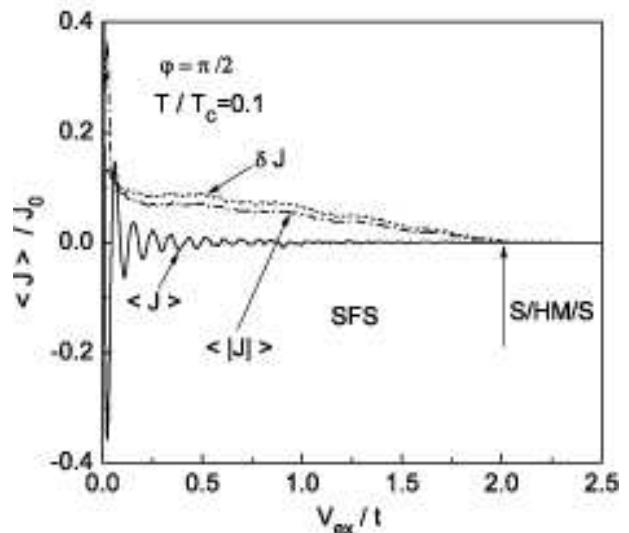


FIG. 2: Josephson current is plotted as a function of the exchange potential V_{ex} for $V_S = 0$ and $\Delta_0 = 0.01t$. At $V_{ex} = 2t$, a ferromagnet becomes half-metallic as indicated by an arrow. The vertical axis is normalized by J_0 which is an ensemble average of Josephson current at $V_{ex} = 0$. The number of samples used for averaging N_s is 500.

sults are normalized by J_0 which is the ensemble averaged of Josephson current in the superconductor / normal metal / superconductor (SNS) junctions (i.e., $V_{ex} = 0$). The Josephson current oscillates as a function of V_{ex} and changes its sign almost periodically. The sign changes of $\langle J \rangle$ correspond to the $0-\pi$ transition of a SFS junction. At the same time, the amplitude of $\langle J \rangle$ decreases rapidly with increasing V_{ex} . For $V_{ex} > 0.1t$, we should pay attention to the relation $\langle J \rangle \ll \delta J$ which means that the

Josephson current is not a self-averaging quantity. It is impossible to predict the Josephson current in a single sample J_i from $\langle J \rangle$ because J_i strongly depends on the microscopic impurity configuration. In fact, the Josephson current flows in *a single sample* even if $\langle J \rangle = 0$ at the transition points. Roughly speaking, $\langle J \rangle$ vanishes because half of samples are 0-junctions and the rest are the π -junctions^{20,26}. Since $\langle J \rangle = 0$, δJ approximately corresponds to the typical amplitude of the Josephson current expected in a single sample. In Fig. 2, we also show $\langle |J| \rangle$, which agrees well with δJ even quantitatively. The relation $\langle J \rangle = 0$ has different meaning for SFS and S/HM/S cases. In a SFS junction, the fact that $\langle J \rangle = 0$ at the transition points is a result of ensemble averaging and the Josephson current remains finite in a single sample. The characteristic temperature and length of a ferromagnet at the $0-\pi$ transitions vary from one sample to another. In S/HM/S junctions at $V_{ex} = 2.5t$, however, $\langle J \rangle = 0$ means that the Josephson current vanishes even in a single sample because $\delta J = 0$ holds at the same time.

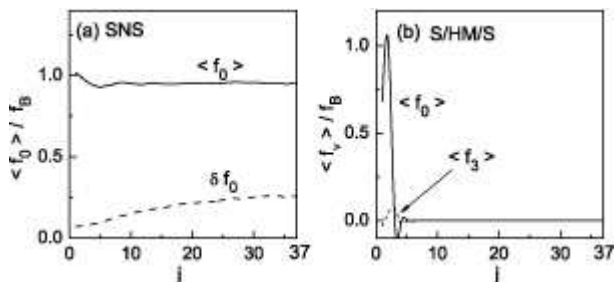


FIG. 3: Pairing functions are plotted as a function of position j for (a) SNS at $V_{ex}/t = 0$ and (b) S/HM/S at $V_{ex}/t = 2.5$, where $V_S = 0$, $\Delta_0 = 0.01t$ and $N_s = 200$. The vertical axis is normalized by a pairing function in a superconductor f_B .

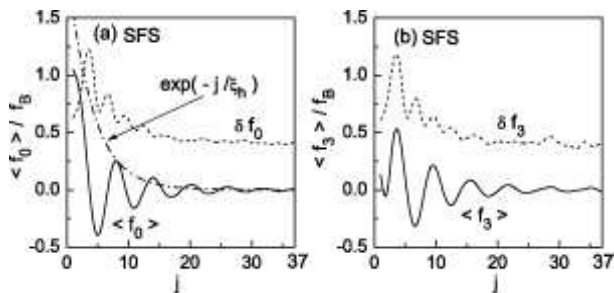


FIG. 4: Pairing functions in SFS junctions with $V_{ex}/t = 1$, $V_S = 0$, $\Delta_0 = 0.01t$ and $N_s = 500$.

The large fluctuations of Josephson current were discussed by Zyuzin et. al.²⁰ by using the diagrammatic expansion. An ensemble average of critical Josephson

current and its fluctuations have a relation for $W \gg L_N$

$$\frac{\delta J}{\langle J \rangle} \sim \sqrt{\frac{1}{W}} \frac{\exp(-L_N/\xi_T)}{\exp(-L_N/\xi_h)}, \quad (14)$$

$$\sim \sqrt{\frac{1}{W}} \exp\left\{(\sqrt{V_{ex}} - \sqrt{\Delta_0})/\sqrt{E_{Th}}\right\}, \quad (15)$$

where $E_{Th} = D/L_N^2$ is the Thouless energy, $\xi_T = \sqrt{D/2\pi T}$, and $\xi_h = \sqrt{D/V_{ex}}$ is estimated to be about four lattice constants (See also Appendix A). In the second line, we replace T by Δ_0 because a measuring temperature must be smaller than T_c . For a weak ferromagnet (i.e., $V_{ex} \lesssim \Delta_0$), the ratio can be less than unity and the Josephson current is a self-averaging quantity. On the other hand, in a strong ferromagnet with $V_{ex} \gg \Delta_0$, the ratio becomes much larger than unity. Thus the large fluctuation of Josephson current is a robust feature of SFS junctions with $V_{ex} \gg \Delta_0$. The only way to suppress fluctuations is taking the junction width sufficiently large because fluctuations are a mesoscopic effect.

The origin of the large fluctuations in the Josephson current can be understood by analyzing pairing functions of Cooper pairs. We plot a pairing function of spin-singlet pairs f_0 in an SNS junction as a function of position in a normal metal j in Fig. 3(a), where $j = 1$ and 37 correspond respectively to the junction interface and the center of the normal metal. The pairing function is calculated for $\varphi = 0$ and is normalized by its bulk value in a superconductor f_B . In SNS junctions, $\langle f_0 \rangle$ is a real value and is almost constant as shown in Fig. 3(a), which means that spin-singlet Cooper pairs exist everywhere in the normal metal. The pairing function for spin-singlet pairs in SFS junctions is shown in Fig. 4(a). An average $\langle f_0 \rangle$ decreases exponentially with j according to $\exp(-j/\xi_h)$. At the same time, $\langle f_0 \rangle$ oscillates in real space and changes its sign. In addition to spin-singlet pairs, opposite-spin-triplet pairs appear in a ferromagnet for $V_{ex} \neq 0$. Since f_3 is a pure imaginary value, the imaginary part of $\langle f_3 \rangle$ is plotted in Fig. 4(b). The behavior of $\langle f_3 \rangle$ is qualitatively the same as that of $\langle f_0 \rangle$ in Fig. 4(a). Thus opposite-spin-triplet pairs also contribute to the Josephson current. Both δf_0 and δf_3 remain finite at the center of a ferromagnet $j = 37$. Spin-singlet and opposite-spin-triplet pairs penetrate deeply into a ferromagnet far beyond ξ_h even though $\langle f_0 \rangle$ and $\langle f_3 \rangle$ are almost zero there. We numerically confirm the relation $\delta f_0 \propto e^{-j/\xi_T}$, in agreement with Ref. 20.

In Fig. 5 (a) and (b), we show f_0 and f_3 in SFS junctions for three samples with different impurity distribution. The vertical axis is shifted as indicated by horizontal lines. The pairing functions are in phase near the interface ($j \leq \xi_h$), whereas they are out of phase far from the interface. Although the pairing function in a sample has a finite value for $j > \xi_h$, an ensemble average of them vanishes. Cooper pairs do exist in *a single sample* of ferromagnet even for $j \gg \xi_h$. Mesoscopic fluctuations of the pairing function provide the origin of the large fluctuations in the Josephson current. In S/HM/S junctions,

as shown in Fig. 3(b), $\langle f_0 \rangle$ and $\langle f_3 \rangle$ vanish for $j \gg 1$. We have also confirmed that $\delta f_0 = \delta f_3 = 0$ for $j \gg 1$ at the same time. Thus, no Cooper pairs exist in a half metal for $V_S = 0$.

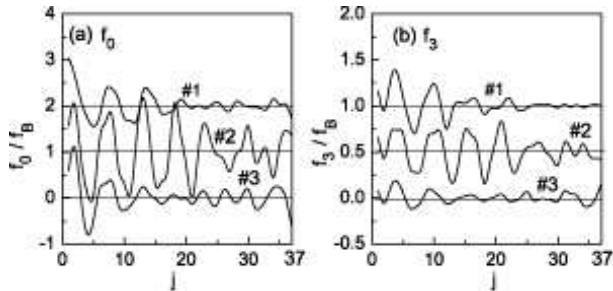


FIG. 5: Pairing functions in three different samples of SFS junction at $V_{ex}/t = 1$.

Since $\langle J \rangle \ll \delta J$, the temperature dependence of Josephson current also depends on the impurity configuration. In Fig. 6, we show the Josephson critical current as a function of temperature for five different samples, where the critical current is estimated from the current-phase relation at each temperature. The solid line in Fig. 6(a) corresponds to a SFS junction in the 0-state, where the critical current monotonically increases with the decrease of temperature. On the other hand, the broken line corresponds to a junction in the π -state. In Fig. 6(b), a junction undergoes the transition from 0 to π state when temperature decreases across $0.5T_c$. On the contrary, the 0-state is more stable than the π -state at low temperatures in Fig. 6(c). The Josephson current is decomposed into a series of $J = \sum_{k=1} J_k \sin(k\varphi)$. In Fig. 6, $J_1 = 0$ characterizes the 0- π transition temperature. At the transition temperature, the critical current is not exactly zero because a higher harmonic such as $J_2 \sin(2\varphi)$ contributes to the Josephson current. Some SFS junctions undergo the 0- π transition twice as shown in Fig. 6(d). The temperature dependence of the critical current in one sample can be very different from that in another samples.

IV. SFS JUNCTION WITH SPIN-ACTIVE INTERFACE

The relation $\langle J \rangle \ll \delta J$ is a characteristic feature of the Josephson current in diffusive SFS junctions with $V_{ex} \gg \Delta_0$. This feature, however, is drastically changed by spin-flip scattering at junction interfaces. In this section, we study the Josephson current in the presence of spin-flip scattering, (i.e., $V_S \neq 0$). In Figs. 7 (a) and (b), we show $\langle J \rangle$ as a function of the spin-flip potential V_S for $V_{ex}/t = 1$ and 2.5, respectively. In both cases (a) and (b), we find that $|\langle J \rangle| \geq \delta J$ for $V_S \geq 0.3t$. The Josephson current recovers the self-averaging property in the presence of spin-flip scattering. Reasons can be found

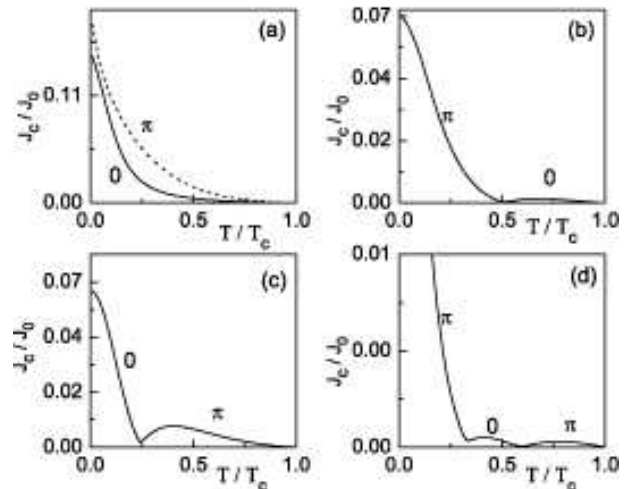


FIG. 6: Critical current versus temperatures for five different samples of SFS junction, where $V_{ex}/t = 1$, $V_S = 0$, and $\Delta_0/t = 0.01$.

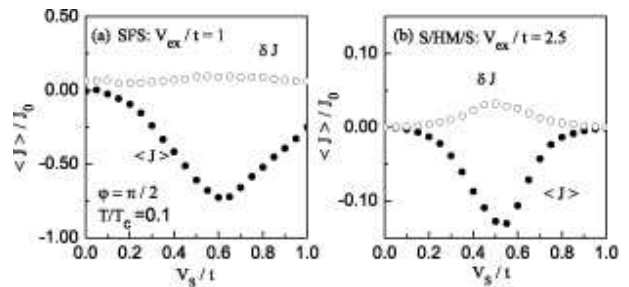


FIG. 7: (a) Josephson current and its fluctuations for $T = 0.1T_c$, $\varphi = \pi/2$ and $N_s = 200$ as a function of interface spin-flip scattering V_S for $V_{ex}/t = 1$ and (b) for $V_{ex}/t = 2.5$. The vertical axis is normalized by an ensemble average of Josephson current at $V_{ex} = 0$ and $V_S = 0$.

by analyzing the pairing functions in a ferromagnet, as shown in Figs. 8 and 9, where four pairing functions are plotted as a function of position j at $V_S/t = 0.4$. In SFS junctions as shown in Fig. 8(a), equal-spin-triplet Cooper pairs penetrate into a ferromagnet by spin-flip scattering at interfaces. Although averages of the pairing function for opposite-spin pairs vanish at $j \sim 37$, their fluctuations remain finite as shown in Figs. 8(a) and (b). Thus four types of Cooper pairs carry the Josephson current in a SFS junction. In a S/HM/S junction, on the other hand, only $\uparrow\uparrow$ -pairs exist in a half metal as shown in Fig. 9(a) and (b). The pairing functions $\langle f_{\downarrow\downarrow} \rangle$, $\langle f_0 \rangle$, and $\langle f_3 \rangle$ vanish for $j \gg 1$. We note that fluctuations of these pairing functions behave similar to their averages. In both SFS and S/HM/S, $\langle f_{\uparrow\uparrow} \rangle$ becomes much larger than δf_0 because the exchange potential does not break down equal-spin-triplet Cooper pairs and $f_{\uparrow\uparrow}$ does not suffer sign change in real space. Thus the Josephson current

becomes a self-averaging quantity as shown in Figs. 7(a) and (b).

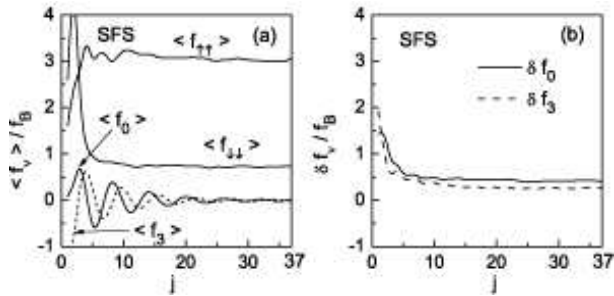


FIG. 8: Pairing functions in SFS junctions are plotted as a junction of j . Ensemble averages and some of their fluctuations are shown in (a) and (b), respectively. The number of samples are taken to be 500.

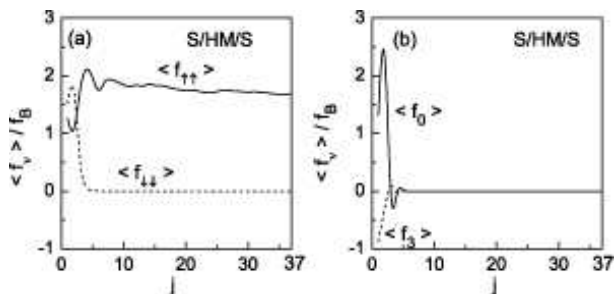


FIG. 9: Pairing functions in S/HM/S junctions are plotted as a junction of j . The number of samples are taken to be 200.

Here we address an unusual symmetry property of Cooper pairs in SFS junctions. In Fig. 10, we show four pairing functions in a SFS junction as a function of ω_n , where $j = 37$, $V_S = 0.2t$, $\varphi = 0$, and $V_{ex} = t$. Although the Green function at $\omega_n = 0$ is not defined, we put $f_{\uparrow\uparrow} = f_{\downarrow\downarrow} = f_3 = 0$ at $\omega_n = 0$, and connect results for positive ω_n with those for negative ω_n . The pairing function f_0 is an even function of ω_n , whereas $f_{\uparrow\uparrow}$, $f_{\downarrow\downarrow}$, and f_3 are an odd function of ω_n ⁶. Since electrons obey Fermi statistics, pairing functions must be antisymmetric under interchanging two electrons,

$$\hat{f}_{\omega_n}(\mathbf{r}, \mathbf{r}') = -[\hat{f}_{-\omega_n}(\mathbf{r}', \mathbf{r})]^t, \quad (16)$$

where $[\hat{f}]^t$ denotes the transpose of \hat{f} meaning the interchange of spins. It is well known that ordinary even-frequency pairs are classified into two symmetry classes: spin-singlet even-parity symmetry and spin-triplet odd-parity one. In the former case, the negative sign on the right hand side of Eq. (16) arises due to the interchange of spins, while in the latter case due to $\mathbf{r} \leftrightarrow \mathbf{r}'$. In the present calculation, all components on the right hand side of Eq. (13) have s -wave symmetry. This is because the

pairing functions are isotropic in both real and momentum spaces due to diffusive impurity scatterings²⁷. As a result, $f_{\uparrow\uparrow}$, $f_{\downarrow\downarrow}$, and f_3 must be an odd function of ω_n to obey Eq. (16). The fraction of odd-frequency pairs depends on parameters such as the exchange potential and the spin-flip potential. As shown Fig. 3(a), all Cooper pairs have even-frequency symmetry in SNS junctions at $V_{ex} = 0$ and $V_S = 0$. Even- and odd-frequency pairs have almost same fraction in SFS junctions at $V_{ex} = t$ and $V_S = 0$ as shown in Fig. 4. In the presence of spin-flip potential, odd-frequency pairs become dominant as shown in Fig. 8. In particular, all Cooper pairs have odd-frequency symmetry in S/HM/S junctions as shown in Fig. 9. The Josephson current in Fig. 7(b) is carried purely by odd-frequency pairs in S/HM/S junctions.

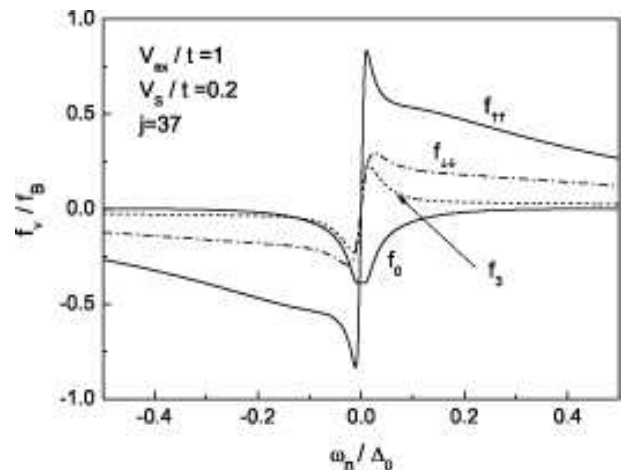


FIG. 10: Pairing functions in a SFS junction are plotted as a junction of ω_n for $V_{ex}/t = 1$ and $V_S/t = 0.2$.

The results in Fig. 7 show that the amplitude of Josephson current first increases with the increase of V_S then decreases. Here we discuss the analytical expression of the Josephson current in S/HM/S junction at $T = 0$,

$$\langle J \rangle = -J_1 \times \left[(\mathbf{V}_L \cdot \mathbf{V}_R - V_L^{(3)} V_R^{(3)}) \sin \varphi + \mathbf{e}_3 \cdot (\mathbf{V}_L \times \mathbf{V}_R) \cos \varphi \right], \quad (17)$$

$$J_1 = \frac{7\zeta(3)}{\pi} e E_{Th} g_N b^2 > 0, \quad (18)$$

$$b = \frac{1}{2} \int_0^{\pi/2} d\gamma \frac{\cos^5 \gamma}{(V_S^2 + \frac{1}{4}) \cos^4 \gamma - V_S^2 \cos^2 \gamma + V_S^4}. \quad (19)$$

Here $\mathbf{V}_R = \sum_{k=1}^3 V_R^{(k)} \mathbf{e}_k$ and $\mathbf{V}_L = \sum_{k=1}^3 V_L^{(k)} \mathbf{e}_k$ are the dimensionless magnetic moments at the right and left junction interface, respectively. We assume that $|\mathbf{V}_R| = |\mathbf{V}_L| = V_S$ and $(e^2/h)g_N$ is the normal conductance of a half metal. Details of derivation are discussed in Appendices A and B. To compare Eq.(17) with the results in Fig. 7(b), we choose $\mathbf{V}_R = \mathbf{V}_L = V_S \mathbf{e}_2$. We also note that the magnetic moment in a half metal

is $\mathbf{V}_{ex} = V_{ex}\mathbf{e}_3$. For $V_S \ll 1$, the amplitude of the Josephson current increases with V_S^2 because $b = 2$ and $\mathbf{V}_L \cdot \mathbf{V}_R - V_L^{(3)}V_R^{(3)} = V_S^2$. In this case, spin-flip scattering assists the Josephson current. For large V_S , on the other hand, the Josephson current decreases proportionally to V_S^{-6} because the spin-flip potential acts like a potential barrier and suppresses the transmission probability of the interface. The Josephson current shows reentrant behavior as shown in Fig. 7. The Josephson current in Fig. 7(b) is calculated at $\varphi = \pi/2$. The results indicate that the S/HM/S junction is a π -junction. This conclusion depends on the direction of the magnetic moments at the spin-flip interfaces. In the case of $\mathbf{V}_L = \mathbf{V}_R$, the Josephson current in Eq. (17) is proportional to $-J_1 \sin \varphi$ in agreement with Fig. 7(b). In the case of antiferromagnetic alignment, $\mathbf{V}_L = -\mathbf{V}_R$, the junction is in the 0-state. Thus we conclude that the stability of the 0-state and that of the π -state depend on the alignment of the magnetic moments at the two interfaces^{28,29}. This feature indicates a new direction to controlling the π -phase shift by using ferromagnetic materials. For $\mathbf{V}_{ex} \cdot (\mathbf{V}_L \times \mathbf{V}_R) \neq 0$, the Josephson current flows even at $\varphi = 0$ because such spin configuration breaks the chiral symmetry of a junction. We have numerically confirmed the Eq. (17).

In the end of this section, we discuss the temperature dependence of the Josephson critical current in SFS and S/HM/S junctions in Fig. 11, where we choose $\Delta_0 = 0.005t$ in connection with the density of states in the next section. The Josephson current has almost a si-

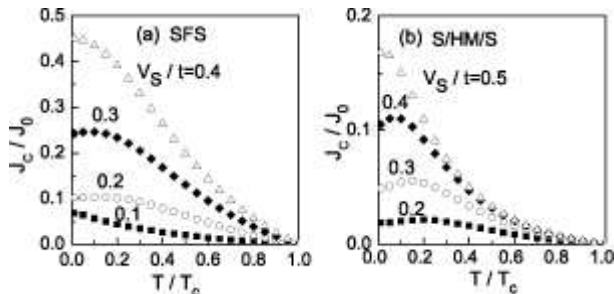


FIG. 11: Temperature dependence of critical Josephson current in SFS (a) and S/HM/S (b) junctions. N_s is taken to be 200.

nusoidal current-phase relationship. The critical current for $V_S/t = 0.2$ and 0.3 in a SFS junction first increases with the decrease of temperature then decreases as shown in Fig. 11(a). Such reentrant behavior is seen more clearly in a S/HM/S junction as shown for $V_S/t = 0.2, 0.3$ and 0.4 in Fig. 11(b). In a Josephson junction consisting of conventional s -wave spin-singlet superconductors, such reentrant behavior is very unusual. This behavior has also been reported in Ref. 16. The results for $V_S/t = 0.4$ in SFS and $V_S/t = 0.5$ in S/HM/S junctions, on the other hand, show a monotonic temperature dependence.

V. DENSITY OF STATES

The proximity effect changes the low energy spectra of a quasiparticle in a normal metal. In a SNS junction, it is well known that the penetration of usual even-frequency spin-singlet s -wave Cooper pairs suppresses the quasiparticle density of states for $E < E_{Th}$. This suppressed density of states is called minigap. In this section, we discuss the proximity effect of odd-frequency pairs on the quasiparticle density of states. In our method, the density of states is given by

$$N(E, j) = -\frac{1}{\pi} \frac{1}{W} \sum_{m=1}^W \text{ImTr} \check{G}_{E+i\gamma}(\mathbf{r}, \mathbf{r}), \quad (20)$$

where γ is a small imaginary part. In Fig. 12, we show the local density of states (LDOS) at $j = 37$ in SFS junctions, where $\varphi = 0$, and $\gamma = 0.1\Delta_0$. The results for S/HM/S junctions are presented in Fig. 13. The LDOS is normalized by its value at $E = 1.2\Delta_0$. Here we choose $\Delta_0 = 0.005t$ so that $E_{Th} \sim 0.3\Delta_0$ is slightly smaller than Δ_0 . In the absence of spin-flip scattering, the ensemble average of LDOS is almost constant in both Figs. 12 and 13. At $V_S/t = 0.3$, the penetration of odd-frequency pairs enhances LDOS for $E < 0.5\Delta_0$. On the other hand, LDOS is suppressed around $E \sim 0.8\Delta_0$ because of a sum rule for the density of states (i.e., $\int dE N(E, j) = \text{const.}$). The low energy spectra of LDOS increase with increasing V_S/t as shown in Figs. 12(b) and 13(b). At $V_S/t = 0.5$, LDOS has a peak at $E = 0$. Thus the penetration of odd-frequency pairs enhances the quasiparticle density of states for $E < E_{Th}$. This tendency is just opposite to the minigap structure due to penetration of even-frequency pairs. The shape of the zero-energy peak in Figs. 12(b) and 13(b) is almost independent of the position in a half metal. The peak is much stronger than the enhancement of the LDOS found in weak ferromagnets^{3,10,30,31,32}. In such SF junctions³¹, the LDOS has an oscillatory peak/dip structure at $E = 0$, which rapidly decays with the distance from the SF interface. Therefore, the large peak at $E = 0$ in the LDOS is a robust and direct evidence of the odd-frequency pairing in a ferromagnet. Scanning tunneling spectroscopy (STS) could be used to detect such a peculiar pairing state.

As shown in Fig. 13, however, the penetration of odd-frequency pairs does not always give rise to a zero-energy peak in LDOS. The results for $V_S/t = 0.3$ and 0.4 have a broad peak at a finite energy smaller than E_{Th} . This situation is slightly different from the large zero-energy peak in a normal metal due to the penetration of odd-frequency pairs from spin-triplet odd-parity superconductors^{33,34,35,36}. In a spin-triplet superconductor junction, LDOS in a normal metal always has a large zero-energy peak because a midgap Andreev resonant state³⁷ assists the zero-bias peak. In ferromagnetic junctions, on the other hand, such a quasiparticle state is absent at the junction interface. The broad peak structure in the LDOS is responsible for the nonmonotonic temper-

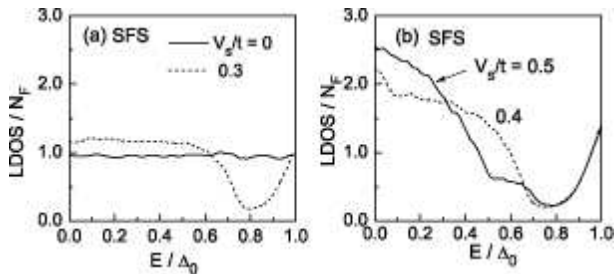


FIG. 12: Local density of states at $j = 37$ in a ferromagnet of SFS junction, where $N_s = 2000$.

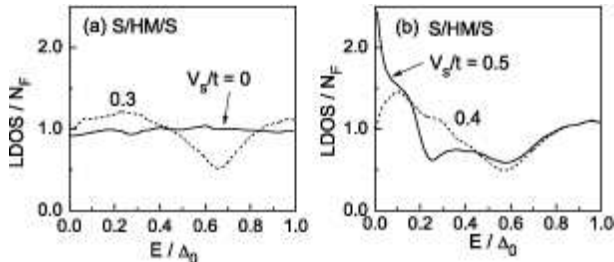


FIG. 13: Local density of states at $j = 37$ in a half metal of S/HM/S junction, where $N_s = 2000$.

ature dependence of the critical current in Fig. 11(b). At high temperatures, quasiparticle states around the peak contribute to the Josephson current. At low temperatures, however, such quasiparticle states cannot contribute to the Josephson current³⁸. We conclude that odd-frequency pairs could also be confirmed by measuring the dependence of the critical current on temperature.

VI. CONCLUSION

In conclusion, we have studied the Josephson effect in superconductor / diffusive ferromagnet / superconductor (SFS) junctions by using the recursive Green function method. When the exchange potential in a ferromagnet is much larger than the pair potential in a superconductor, the Josephson current is not a self-averaging quantity. This is because spin-singlet Cooper pairs penetrating into a ferromagnet far beyond ξ_h cause large fluctuations of the pairing function. As a consequence, the temperature dependence of the critical Josephson current in one sample can be very different from that in another sample. When a ferromagnet is half-metallic, the Josephson current vanishes in the absence of spin-flip scattering at junction interfaces. Spin-flip scattering at interfaces allows equal-spin-triplet odd-frequency Cooper pairs to penetrate into a ferromagnet. The ratio of odd-frequency pairs to even-frequency ones depends on the exchange potential in a ferromagnet and the spin-flip potential at interfaces. The Josephson current recovers

the self-averaging property when the fraction of equal-spin-triplet pairs becomes large. In half-metallic SFS junctions, all Cooper pairs have odd-frequency symmetry. The penetration of odd-frequency pairs enhances low energy quasiparticle density of states in a ferromagnet. Such low energy spectra could be probed by scanning tunneling spectroscopy and determining a nonmonotonic temperature dependence of the critical Josephson current. We also discuss a way to realize a π -junction by controlling magnetic moments in ferromagnetic layers.

Acknowledgments

We acknowledge helpful discussions with J. Aarts, T. M. Klapwijk, G. E. W. Bauer, Yu. V. Nazarov, S. Maekawa, S. Takahashi, A. I. Buzdin, A. F. Volkov and A. Brinkman. This work was partially supported by the Dutch FOM, the NanoNed program under grant TCS7029 and Grant-in-Aid for Scientific Research from The Ministry of Education, Culture, Sports, Science and Technology of Japan (Grant No. 19540352, 18043001, 17071007 and 17340106).

APPENDIX A: FLUCTUATIONS OF JOSEPHSON CURRENT

The purpose of this appendix is to explain Eq. (14). Since fluctuations of Josephson current have been calculated by the diagrammatic expansion^{19,20,39}, we also calculate the Josephson current in SFS junctions in the same method. We assume that relations $E_{Th} \ll \Delta_0$, $V_{ex} \ll \mu$ and $L_N \gg \ell$ are satisfied. In the lowest coupling, the Josephson current is given by a formula⁴⁰

$$J = ie \sum_{l,r} T \sum_{\omega_n} \text{Tr} [\hat{r}_l^{eh} \cdot \hat{t}_{lr}^h \cdot \hat{r}_r^{he} \cdot \hat{t}_{rl}^e - \hat{r}_l^{he} \cdot \hat{t}_{lr}^e \cdot \hat{r}_r^{eh} \cdot \hat{t}_{rl}^h], \quad (\text{A1})$$

where l (r) denotes a propagating channel at the left (right) junction interface. In Fig. 14(a), a propagation process of the first term in Eq. (A1) is schematically illustrated. We calculate the transmission coefficients in a ferromagnet such as \hat{t}_{rl}^e and \hat{t}_{lr}^h and Andreev reflection coefficients at interfaces such as \hat{r}_r^{he} and \hat{r}_l^{eh} by parts. The Andreev reflection coefficients are calculated at an ideal NS interface as shown in the left figure of Fig. 14(b). The results are given by

$$\hat{r}_{l(r)}^{he} = -\hat{\sigma}_2 \frac{\Delta_0}{\omega_n + \Omega_n} e^{-i\varphi_{L(R)}}, \quad (\text{A2})$$

$$\hat{r}_{l(r)}^{eh} = \hat{\sigma}_2 \frac{\Delta_0}{\omega_n + \Omega_n} e^{i\varphi_{L(R)}}, \quad (\text{A3})$$

where $\Omega_n = \sqrt{\omega_n^2 + \Delta_0^2}$. The effect of the exchange potential is considered through transmission coefficients of

an electron in a ferromagnet

$$\hat{t}_{lr}^e = \begin{pmatrix} t_{lr}^{e,(\uparrow)} & 0 \\ 0 & t_{lr}^{e,(\downarrow)} \end{pmatrix}. \quad (\text{A4})$$

The transmission coefficients of a hole are defined in the same way by $e \rightarrow h$ in the equation above. The transmission coefficients are represented by the Green function as

$$t_{rl}^e(\sigma) = ie^{ik_l x_L - ik_r x_R} v_l \iint dy_L dy_R Y_r^*(y_R) Y_l(y_L) \times G_{\omega_n}^\sigma(x_R, y_R; x_L, y_L) \quad (\text{A5})$$

$$t_{rl}^h(\sigma) = -ie^{-ik_l x_L + ik_r x_R} v_r \iint dy_L dy_R Y_l^*(y_L) Y_r(y_R) \times G_{-\omega_n}^\sigma(x_R, y_R; x_L, y_L), \quad (\text{A6})$$

where $Y_l(y)$ is a wave function in the y direction and $v_l = k_l/m$ with k_l being a wave number in the x direction on the Fermi surface in the l th propagating channel. In above expression, we have assumed that two ideal lead wires are attached to the both sides of a diffusive ferromagnet, and $x_L < 0$ and $(x_R > L_N)$ are taken to be in the lead wires. The Green function is given by

$$G_{\omega_n}^\sigma(\mathbf{r}, \mathbf{r}') = \frac{1}{(2\pi)^2} \int \frac{d\mathbf{k}}{i\omega_n - \xi_k + V_{ex}s + \frac{i}{2\tau} \text{sgn}(\omega_n)}, \quad (\text{A7})$$

where τ is the elastic mean free time, $\xi_k = \mathbf{k}^2/m - \mu$, and $s = 1(-1)$ for $\sigma = \uparrow(\downarrow)$. An ensemble average of transmission coefficients is calculated by the diagrammatic expansion

$$\sum_{lr} \langle t_{lr}^e(\sigma) t_{rl}^h(\sigma') \rangle = \frac{v_F^2}{2} \int_0^W dy_L \int_0^W dy_R P_C^{\sigma\sigma'}(L + \delta, y_R; -\delta, y_L; 2\omega_n), \quad (\text{A8})$$

$$P_C^{\sigma\sigma'}(\mathbf{r}, \mathbf{r}') = \langle G_{\omega_n}^\sigma(\mathbf{r}, \mathbf{r}') G_{-\omega_n}^{\sigma'}(\mathbf{r}, \mathbf{r}') \rangle, \quad (\text{A9})$$

where $P_C^{\sigma\sigma'}$ is the Cooperon propagator which satisfies the equation

$$[|\omega_l| - 2iV_{ex}s(1 - \delta_{\sigma,\sigma'}) - D\nabla^2] P_{C,D}^{\sigma\sigma'}(\mathbf{r}, \mathbf{r}'; \omega_l) = 2\pi N_0 \delta(\mathbf{r} - \mathbf{r}'). \quad (\text{A10})$$

Since $\mu \gg V_{ex}$, the diffusion constant D , the Fermi velocity v_F and the density of states at the Fermi energy N_0 do not depend on spin directions. In Fig. 14(c), we illustrate the Cooperon and diffuson propagator, where $\omega_l = 2\pi lT$ is a boson Matsubara frequency. In Fig. 14(d) we show two diagrams which contribute to the Josephson current. The left (right) diagram in Fig. 14(d) corresponds to the first (second) term of Eq. (A1). Only $P_C^{\uparrow\downarrow}$ and $P_C^{\downarrow\uparrow}$ contribute to the Josephson current because the Andreev reflection coefficients are off-diagonal in spin space. To calculate the Cooperon propagator, we solve the diffusion

equation with appropriate boundary conditions²⁶

$$D\nabla^2 h_\lambda(\mathbf{r}) = \lambda h_\lambda(\mathbf{r}), \quad (\text{A11})$$

$$h_\lambda(\mathbf{r})|_{x=0, L_N} = 0, \quad (\text{A12})$$

$$\left. \frac{\partial h_\lambda(\mathbf{r})}{\partial y} \right|_{y=0, W} = 0. \quad (\text{A13})$$

The Cooperon propagator is represented by using wave functions and their eigen values of the diffusion equation. The results are

$$P_C^{\sigma\sigma'}(\mathbf{r}, \mathbf{r}'; 2\omega_n) = 2\pi N_0 \sum_{n=1}^{\infty} \sum_{m=0}^{\infty} \left(\frac{2}{L_N} \right) B_m \times \frac{\sin(p_n x) \sin(p_n x') \cos(\nu_m y) \cos(\nu_m y')}{2\{|\omega_n| - iV_{ex}s(1 - \delta_{\sigma,\sigma'})\} + D(p_n^2 + \nu_m^2)}, \quad (\text{A14})$$

$$p_n = \frac{n\pi}{L_N}, \quad \nu_m = \frac{m\pi}{W}, \quad (\text{A15})$$

$$B_m = \begin{cases} 1/W & \text{for } m = 0 \\ 2/W & \text{for } m \neq 0, \end{cases} \quad (\text{A16})$$

By substituting the above results into Eq. (A8), we arrive at

$$\sum_{lr} \langle t_{lr}^e(\sigma) t_{rl}^h(\bar{\sigma}) \rangle = g_N \left(\frac{\eta^{\sigma\bar{\sigma}}}{\sinh \eta^{\sigma\bar{\sigma}}} \right), \quad (\text{A17})$$

$$g_N = \pi N_0 DW / L_N, \quad (\text{A18})$$

$$\eta^{\sigma\sigma'} = \begin{cases} \sqrt{\frac{2|\omega_n| - 2isV_{ex}}{E_{Th}}} & \sigma' = \bar{\sigma} \\ \sqrt{\frac{2|\omega_n|}{E_{Th}}} & \sigma' = \sigma \end{cases}, \quad (\text{A19})$$

where $(2e^2/h)g_N$ is the conductance of a ferromagnet, $\bar{\sigma}$ denotes the opposite spin state of σ , and integration in the y direction in Eq. (A8) is carried out at $\delta = \ell/\sqrt{2}$. The Josephson current becomes

$$\langle J \rangle = 2e g_N \sin \varphi T \sum_{\omega_n} \sum_{\sigma} \frac{\eta^{\sigma\bar{\sigma}}}{\sinh \eta^{\sigma\bar{\sigma}}} \left[\frac{\Delta_0}{\omega_n + \Omega_n} \right]^2. \quad (\text{A20})$$

By substituting equations

$$\sum_{\sigma} \frac{\eta^{\sigma\bar{\sigma}}}{\sinh \eta^{\sigma\bar{\sigma}}} = 4 \sqrt{\frac{2V_{ex}}{E_{Th}}} e^{-\frac{L_N}{\xi_h}} \sin \left(\frac{L_N}{\xi_h} + \frac{\pi}{4} \right), \quad (\text{A21})$$

$$T \sum_{\omega_n} \left(\frac{\Delta_0}{\omega_n + \Omega_n} \right)^2 = \frac{2\Delta_0}{3\pi}, \quad (\text{A22})$$

into above expression, the Josephson current at $T = 0$ results in

$$\langle J \rangle = \frac{16\sqrt{2}}{3\pi} e g_N \Delta_0 \sqrt{\frac{V_{ex}}{E_{Th}}} e^{-\frac{L_N}{\xi_h}} \sin \left(\frac{L_N}{\xi_h} + \frac{\pi}{4} \right) \times \sin \varphi. \quad (\text{A23})$$

This expression is also valid for $V_{ex} \lesssim \Delta_0$ because the relation $V_{ex} \gg \Delta_0$ was not explicitly used in the derivation.

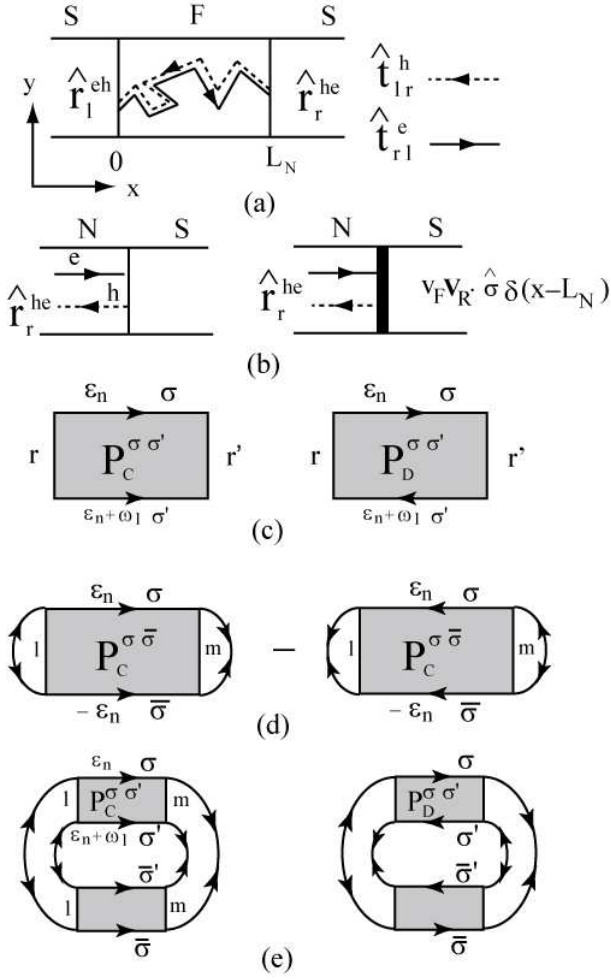


FIG. 14: (a): a propagation process of a quasiparticle in a SFS junction. We describe the Andreev reflection coefficients in Eq. (A1) by those at an ideal normal-metal/superconductor interface as shown in (b). (c): Cooperon and diffuson propagator. The diagrams for Josephson current (d) and its fluctuations (e).

In Fig 14(e), we show two typical diagrams for fluctuations. Not only $P^{\sigma\bar{\sigma}}$ but also $P^{\sigma\sigma}$ contributes to fluctuations. The Cooperon $P^{\sigma\bar{\sigma}}$ behaves like e^{-L_N/ξ_h} similar to the Josephson current. On the other hand, $P^{\sigma\sigma} \sim e^{-L_N/\xi_T}$. Thus amplitude of fluctuations in SFS junctions is almost the same as that in SNS junctions. Our approach, however, is not suitable for calculating fluctuations because a number of diagrams contributes to fluctuations in addition to Fig. 14(e). Here we present the result for SNS junctions at $T = 0$ and $\varphi = \pi/2$ obtained by a slightly different approach³⁹

$$\delta J = \sqrt{\frac{\pi}{6}} e E_{Th} \sqrt{\frac{W}{L_N}}. \quad (\text{A24})$$

The fluctuations in SFS junctions are given by $\delta J/\sqrt{2}$ because contribution of $P^{\sigma,\bar{\sigma}}$ is negligible for $V_{ex} \gg E_{Th}$.

Thus the ratio is described by

$$\frac{\delta J}{\langle J \rangle} \sim \frac{\sqrt{6\pi^3}}{16} \sqrt{\frac{L_N}{W}} \frac{1}{k_F \ell} e^{L_N/\xi_h} \frac{E_{Th}^{3/2}}{\Delta_0 \sqrt{V_{ex}}}. \quad (\text{A25})$$

Since $P^{\sigma\sigma} \sim e^{-L_N/\xi_T}$, temperature dependence of fluctuations is also expected to be e^{-L_N/ξ_T} . Thus we arrive at Eq. (14). In a recent paper, mesoscopic fluctuations of the Josephson current were calculated within the quasiclassical Green function technique⁴¹. In this approach the fluctuations are slightly larger than those within the diagrammatic expansion^{19,39}. The difference may stem from the proximity effect on electronic structure in a normal metal such as the minigap in the quasiparticle density of states. In the diagrammatic expansion, such effect is not taken into account.

APPENDIX B: NEGATIVE JOSEPHSON COUPLING

Here we express the Josephson current in S/HM/S junctions with spin-active interface on the basis of the diagrammatic expansion. In a half metal, we assume that the magnetic moment is parallel to e_3 . Thus transmission coefficients of an electron become

$$\hat{t}_{rl}^e = \frac{\hat{\sigma}_0 + \hat{\sigma}_3}{2} t_{rl}^e(\uparrow) \quad (\text{B1})$$

because electric structure for \downarrow spin is insulating in a half metal. Transmission coefficients of a hole are defined in the same way by $e \rightarrow h$. Andreev reflection coefficients \hat{r}_r^{he} and \hat{r}_r^{eh} in Eq. (A1) are calculated at a normal-metal/superconductor interface at which a spin-flip potential $v_F \mathbf{V}_R \cdot \hat{\sigma} \delta(x - L_N)$ is introduced as shown in the right figure of Fig. 14(b). Andreev reflection coefficients \hat{r}_l^{he} and \hat{r}_l^{eh} are also calculated at a normal-metal/superconductor interface at which a spin-flip potential $v_F \mathbf{V}_L \cdot \hat{\sigma} \delta(x)$ is considered. We assume that $\mathbf{V}_{L(R)} = \sum_{k=1}^3 V_{L(R)}^{(k)} \mathbf{e}_k$ and $|\mathbf{V}_L| = |\mathbf{V}_R| = V_S$. The calculated results of Andreev reflection coefficients are given by

$$\hat{r}_l^{he} = -Q_l \hat{\sigma}_2 [A_l \hat{\sigma}_0 + i B_l \mathbf{V}_L \cdot \hat{\sigma}] e^{-i\varphi_L}, \quad (\text{B2})$$

$$\hat{r}_l^{eh} = Q_l [A_l \hat{\sigma}_0 + i B_l \mathbf{V}_L \cdot \hat{\sigma}] \hat{\sigma}_2 e^{i\varphi_L}, \quad (\text{B3})$$

$$Q_l = \frac{\Delta_0}{A_l^2 + V_S^2 B_l^2} \frac{q_l^2}{2}, \quad (\text{B4})$$

$$A_l = -\Omega_n V_S^2 + q_l^2 \frac{(\Omega_n + \omega_n)}{2}, \quad (\text{B5})$$

$$B_l = q_l (\Omega_n + \omega_n), \quad (\text{B6})$$

where $q_l = k_l/k_F > 0$ are normalized wave number of the l th propagating channel in the current direction. Andreev reflection coefficients at the right interface \hat{r}_r^{he} and \hat{r}_r^{eh} are also obtained by $l \rightarrow r$, $\mathbf{V}_L \rightarrow \mathbf{V}_R$, and $\varphi_L \rightarrow \varphi_R$ in above expression. Since the half metal is in the diffusive transport regime, transmission coefficients

across the half metal, namely \hat{t}_{lr}^e , \hat{t}_{rl}^e , \hat{t}_{lr}^h , and \hat{t}_{rl}^h are independent of propagating channels l and r . Thus average of the Andreev reflection coefficients over all propagating channels contribute to the Josephson current²⁶. We define such Andreev reflection coefficients as

$$\hat{r}_{l(r)}^{he} = \frac{1}{N_c} \sum_{l(r)} \hat{r}_{l(r)}^{he}, \quad (\text{B7})$$

$$= -\hat{\sigma}_2 [a\hat{\sigma}_0 + ib\mathbf{V}_{L(R)} \cdot \hat{\boldsymbol{\sigma}}] e^{-i\varphi_{L(R)}}, \quad (\text{B8})$$

$$\hat{r}_{l(r)}^{eh} = \frac{1}{N_c} \sum_{l(r)} \hat{r}_{l(r)}^{eh}, \quad (\text{B9})$$

$$= [a\hat{\sigma}_0 + ib\mathbf{V}_{L(R)} \cdot \hat{\boldsymbol{\sigma}}] \hat{\sigma}_2 e^{i\varphi_{L(R)}}, \quad (\text{B10})$$

where $N_c = Wk_F/\pi$ is the number of propagating channels at Fermi energy, a and b are real numbers depending only on ω_n , Δ_0 , and V_S . A part of Eq. (A1) becomes

$$I_1 = \sum_{l,r} \langle \text{Tr}[\hat{r}_l^{eh} \cdot \hat{t}_{lr}^h \cdot \hat{r}_r^{he} \cdot \hat{t}_{rl}^e] \rangle, \quad (\text{B11})$$

$$= - \sum_{l,r} \langle \hat{t}_{lr}^h(\uparrow) \hat{t}_{rl}^e(\uparrow) \rangle \frac{e^{i\varphi}}{4} \text{Tr} [(a + ib\mathbf{V}_R \cdot \hat{\boldsymbol{\sigma}}) \times (\hat{\sigma}_0 - \hat{\sigma}_3)(a + ib\mathbf{V}_L \cdot \hat{\boldsymbol{\sigma}})(\hat{\sigma}_0 + \hat{\sigma}_3)], \quad (\text{B12})$$

$$= e^{i\varphi} b^2 g_N \frac{\eta^{\uparrow\uparrow}}{\sinh \eta^{\uparrow\uparrow}} \times [\mathbf{V}_L \cdot \mathbf{V}_R - V_L^{(3)} V_R^{(3)} + ie_3 \cdot (\mathbf{V}_R \times \mathbf{V}_L)], \quad (\text{B13})$$

where we used Eq. (A17). In the same way, we obtain

$$I_2 = \sum_{l,r} \langle \text{Tr}[\hat{r}_r^{eh} \cdot \hat{t}_{rl}^h \cdot \hat{r}_l^{he} \cdot \hat{t}_{lr}^e] \rangle, \quad (\text{B14})$$

$$= e^{-i\varphi} b^2 g_N \frac{\eta^{\uparrow\uparrow}}{\sinh \eta^{\uparrow\uparrow}} \times [\mathbf{V}_L \cdot \mathbf{V}_R - V_L^{(3)} V_R^{(3)} - ie_3 \cdot (\mathbf{V}_R \times \mathbf{V}_L)]. \quad (\text{B15})$$

As a result, the expression for the Josephson takes the form

$$\langle J \rangle \approx -J_1 \left[(\mathbf{V}_L \cdot \mathbf{V}_R - V_L^{(3)} V_R^{(3)}) \sin \varphi + e_3 \cdot (\mathbf{V}_L \times \mathbf{V}_R) \cos \varphi \right], \quad (\text{B16})$$

$$J_1 = 2e g_N T \sum_{\omega_n} \frac{\eta^{\uparrow\uparrow}}{\sinh \eta^{\uparrow\uparrow}} b^2 > 0. \quad (\text{B17})$$

The Josephson current is zero in the absence of spin-flip scattering at the interface (i.e., $\mathbf{V}_L = \mathbf{V}_R = 0$). We note that the ratio $\eta^{\uparrow\uparrow}/\sinh \eta^{\uparrow\uparrow}$ rapidly decreases to zero for $\omega_n/E_{Th} \gg 1$, whereas ω_n dependence of b is scaled by Δ_0 . For $E_{Th} \ll \Delta_0$, we find at $T = 0$

$$J_1 = \frac{7\zeta(3)}{\pi} e E_{Th} g_N b^2, \quad (\text{B18})$$

$$b = \frac{1}{2} \int_0^{\pi/2} d\gamma \frac{\cos^5 \gamma}{(V_S^2 + \frac{1}{4}) \cos^4 \gamma - V_S^2 \cos^2 \gamma + V_S^4}. \quad (\text{B19})$$

Although Eq. (B16) describes well the dependence of the Josephson current on \mathbf{V}_L and \mathbf{V}_R , it does not explain the nonmonotonic temperature dependence of the critical current shown in Fig. 11(b). This is because the proximity effect on the density of states in a half metal is not taken into account in the above estimate.

¹ P. Fulde and R. A. Ferrell, Phys. Rev. **135**, A550 (1964).

² A. I. Larkin and Y. N. Ovchinnikov, Sov. Phys. JETP **20**, 762 (1965).

³ A. I. Buzdin, L. N. Bulaevskii, and S. V. Panyukov, JETP Lett. **35**, 179 (1982).

⁴ A. I. Buzdin, Rev. Mod. Phys. **77**, 935 (2005).

⁵ V. T. Petrashov, V. N. Antonov, S. Maksimov, and R. Shaikhaidarov, JETP Lett. **59**, 551 (1994).

⁶ F. S. Bergeret, A. F. Volkov, and K. B. Efetov, Phys. Rev. Lett. **86**, 4096 (2001); Rev. Mod. Phys. **77**, 1321 (2005).

⁷ A. Kadigrobov, R. I. Shekhter, and M. Jonson, Europhys. Lett. **54**, 394 (2001).

⁸ V. V. Ryazanov, V. A. Oboznov, A. Yu. Rusanov, A. V. Veretennikov, A. A. Golubov, and J. Aarts, Phys. Rev. Lett. **86**, 2427 (2001).

⁹ T. Kontos, M. Aprili, J. Lesueur, F. Genet, B. Stephanidis, and R. Boursier, Phys. Rev. Lett. **89**, 137007 (2002).

¹⁰ A. A. Golubov, M. Yu. Kupriyanov, and E. Ilichev, Rev. Mod. Phys. **76**, 411 (2004).

¹¹ K. Usadel, Phys. Rev. Lett. **25**, 507 (1970).

¹² J. W. A. Robinson, S. Piano, G. Burnell, C. Bell, and M. G. Blamire, Phys. Rev. Lett. **97**, 177003 (2006).

¹³ R. S. Keizer, S. T. B. Goennenwein, T. M. Klapwijk, G. Miao, G. Xiao, A. Gupta, Nature **439**, 825 (2006).

¹⁴ Y. Asano, Y. Tanaka, and A. A. Golubov, Phys. Rev. Lett. **98**, 107002 (2007).

¹⁵ V. Braude and Yu. V. Nazarov, Phys. Rev. Lett. **98**, 077003 (2007).

¹⁶ M. Eschrig and T. Lofwander, cond-mat/0612533.

¹⁷ S. Takahashi, S. Hikino, M. Mori, J. Martinek, and S. Maekawa, Phys. Rev. Lett. **99**, 057003 (2007); S. Hikino, S. Takahashi, M. Mori, J. Martinek and S. Maekawa, Physica C **463-465**, 198 (2007).

¹⁸ M. Eschrig, J. Kopu, J. C. Cuevas, and G. Schon, Phys.

- Rev. Lett. **90**, 137003 (2003).
- ¹⁹ B. Al'tshuler and B. Z. Spivak, Sov. Phys. JETP **65**, 343 (1987).
- ²⁰ A. Yu. Zyuzin, B. Spivak, and M. Hruska, Europhys. Lett. **62**, 97 (2003).
- ²¹ P. G. de Gennes, *Superconductivity of Metals and Alloys*, (Benjamin, New York, 1966).
- ²² A. Furusaki, Physica B. **203**, 214 (1994).
- ²³ Y. Asano, Phys. Rev. B **63**, 052512 (2001).
- ²⁴ G. Eilenberger, Z. Phys. **214**, 195 (1968).
- ²⁵ In two-dimensional lattices, wave function of a quasiparticle is basically localized due to random impurity potential. In the present parameter choice, the localization length ξ_{AL} and the mean free path ℓ at $V_{ex} = 0$ are estimated about 90 and 6 lattice constant, respectively. We have confirmed that these values are not so much sensitive to V_{ex} . The present parameter choice enables us to study transport in the diffusive transport regime because a relation $\ell \ll L_N < \xi_{AL}$ is satisfied. Effects of the localization on Josephson current are important when we choose $L_N \gg \xi_{AL}$ ³⁸.
- ²⁶ Y. Asano, Phys. Rev. B **64**, 014511 (2001); J. Phys. Soc. Jpn. **71**, 905 (2002).
- ²⁷ Y. Tanaka and A. A. Golubov, Phys. Rev. Lett. **98**, 037003 (2007).
- ²⁸ A. F. Volkov, F. S. Bergeret, and K. B. Efetov, Phys. Rev. Lett. **90**, 117006 (2003).
- ²⁹ After submission, we have learned of a recent paper by M. Houzet and A. I. Buzdin, (Phys. Rev. B **76**, 060504(R) (2007)) which gives the same conclusion.
- ³⁰ M. Fogelstrom, Phys. Rev. B **62**, 11812 (2000).
- ³¹ T. Kontos, M. Aprili, J. Lesueur, and X. Grison, Phys. Rev. Lett. **86**, 304 (2001).
- ³² T. Yokoyama, Y. Tanaka, and A. A. Golubov, Phys. Rev. B **72**, 052512 (2005).
- ³³ Y. Tanaka and S. Kashiwaya, Phys. Rev. B **70**, 012507 (2004); Y. Tanaka, S. Kashiwaya, and T. Yokoyama, Phys. Rev. B **71**, 094513 (2005).
- ³⁴ Y. Tanaka, Y. Asano, A. A. Golubov, and S. Kashiwaya, Phys. Rev. B **72**, 140503(R) (2005).
- ³⁵ Y. Asano, Y. Tanaka, and S. Kashiwaya, Phys. Rev. Lett. **96**, 097007 (2006).
- ³⁶ Y. Asano, Y. Tanaka, A. A. Golubov, and S. Kashiwaya, Phys. Rev. Lett. **99**, 067005 (2007).
- ³⁷ Y. Tanaka and S. Kashiwaya, Phys. Rev. Lett. **74**, 3451 (1995).
- ³⁸ Y. Asano, Phys. Rev. B **66**, 174506 (2002).
- ³⁹ Y. Koyama, Y. Takane, and H. Ebisawa, J. Phys. Soc. Jpn. **66**, 430 (1997).
- ⁴⁰ Y. Asano, Phys. Rev. B **64**, 224515 (2001).
- ⁴¹ M. Houzet and M. A. Skvortsov, arXiv:0704.3436.